Available online at www.scholarsresearchlibrary.com

Scholars Research Library

Archives of Applied Science Research, 2013, 5 (2):109-120
(http://scholarsresearchlibrary.com/archive.html)

ISSN 0975-508X
CODEN (USA) AASRC9

The scattering coefficient, extinction coefficient and single scattering albedo of water soluble in the radiative forcing of urban aerosols

D. O. Akpootu and M. Momoh

Department of Physics, Usmanu Danfodiyo University, Sokoto

ABSTRACT

In this paper, the optical depths, scattering coefficient, absorption coefficient, extinction coefficient and single scattering albedo were modeled using Optical Properties of Aerosols and Clouds (OPAC) by slightly altering the number densities of water soluble at spectral range of 0.25 – 1.00 μm for eight different relative humidities (RHs) (0, 50, 70, 80, 90, 95, 98 and 99 %). The data was used to calculate the radiative forcing (RF). The RF was observed to decrease at all RHs given rise to negative RF when compared, as we moved from the first model to the fifth model reflecting the dominance of cooling effect. The scattering coefficient as well as the extinction coefficients and single scattering albedo increases with RHs attributing to a more scattering aerosol. The regression analysis of the Ångström exponents and curvatures which helps in determining the sizes of atmospheric particles was done using SPSS 16.0 software. The analysis reveals that fine mode particles are dominant.

Key words: Scattering coefficient, extinction coefficient, single scattering albedo, water soluble, radiative forcing, urban aerosols.

INTRODUCTION

Aerosols have a direct radiative forcing because they scatter and absorb solar and infrared radiation in the atmosphere. Aerosols also alter the formation and precipitation efficiency of liquid-water, ice and mixed-phase clouds, thereby causing an indirect radiative forcing associated with these changes in cloud properties [25]. The direct and indirect effects of atmospheric aerosols on radiative forcing and cloud physics are strongly dependent on particle size characteristics and chemical compositions [18-20].

Light scattering by aerosols particles result in a negative radiative forcing (cooling effect), as part of the solar flux is scatter back to space. If the particles contain absorbing material, total forcing can become positive (heating effect or warming effect), as the energy absorbed by the particles leads to an increase of thermal radiation [17].

The net effect of aerosols on global climate change is uncertain since the effect of particles can be to cool or to warm, depending on their optical properties. The reduction in the intensity of a direct solar beam during its propagation through the atmosphere is determined by absorption and scattering processes. The aerosol single scattering albedo, $\omega_0$is one of the most relevant optical properties of aerosols, since their direct radiative effect is very sensitive to it. The extinction coefficient, γ, is defined as the sum of absorption coefficient, α and scattering coefficient, β [24] as

$$\gamma(\lambda) = \alpha(\lambda) + \beta(\lambda) \qquad (1)$$

The aerosol single scattering albedo, ω_0 is defined as the fraction of the aerosol light scattering over the extinction as

$$\omega_0 = \frac{\beta(\lambda)}{\gamma(\lambda)} \quad (2)$$

Sulphate and nitrate aerosols which are contained in water soluble from anthropogenic sources, are considered the primary particles responsible for net cooling. They scatter solar radiation and are effective as cloud condensation nuclei affecting the lifetime of clouds, the hydrological cycle and resulting in a negative radiative forcing that leads to a cooling of the Earth's surface. To some extent, they are thought to counteract global warming caused by greenhouse gases such as carbon (iv) oxide [4]. On the other hand, light-absorbing particles, mainly formed by black carbon produced by incomplete combustion of carbonaceous fuels are effective absorbers of solar radiation and have therefore the opposite effect i.e. they warm the atmosphere. Absorption of solar radiation by aerosols causes heating of the lower troposphere, which may lead to altered vertical stability, with implications for the hydrological cycle [26].

The aim of this paper is to calculate and analyze the effect of water soluble in the RF of urban aerosols at spectral range of 0.25 – 1.00 μm. The spectral behaviour of optical parameters analysed are the scattering coefficient, extinction coefficient and single scattering albedo which help in determining the nature of the aerosols. The Ångström exponents and curvatures were also analyzed to determine the fine and coarse mode particles along with the turbidity coefficient.

MATERIALS AND METHODS

The models extracted from OPAC are given in table 1.

Table 1: Compositions of aerosols types [21].

Components	Model 1	Model 2	Model 3	Model 4	Model 5
	No.density (cm^{-3})	No.density (cm^{-3})	No.density (cm^{-3})	No.density (cm^{-3})	No.density (cm^{-3})
Insoluble	1.50	1.50	1.50	1.50	1.50
water soluble	15,000.00	20,000.00	25,000.00	30,000.00	35,000.00
Soot	120,000.00	120,000.00	120,000.00	120,000.00	120,000.00
Total	135,001.50	140,001.50	145,001.50	150,001.50	155,001.50

The data used for the urban aerosols in this paper are derived from the Optical Properties of Aerosols and Clouds (OPAC) data set [21]. In this, a mixture of three components is used to describe Urban aerosols: a water soluble (WASO) components consist of scattering aerosols that are hygroscopic in nature, such as sulphates and nitrates present in anthropogenic pollution, water insoluble (INSO) and Soot.

To estimate the radiative forcing, we adopt the approach used by [6] where they show that the direct aerosol radiative forcing ΔF_R at the top of the atmosphere can be approximated by:

$$\Delta F_R = -\frac{S_0}{4} T_{atm}^2 (1 - N_{cloud}) 2\tau\{(1-a)^2 \beta\omega - 2a(1-\omega)\} \quad (3)$$

where S_0 is the solar constant, T_{atm} is the transmittance of the atmosphere above the aerosol layer, N_{cloud} is the fraction of the sky covered by clouds,τ is the aerosol optical depth, ω is the average single scattering albedo of the aerosol layer, a is the albedo of the underlying surface and β is the fraction of radiation scattered by aerosol into the atmosphere [25]. The upscattering fraction is calculated using an approximate relation [28]

$$\beta = \frac{1}{2}(1 - g) \quad (4)$$

where g is the asymmetry parameter of the aerosol layer. The model parameters are assigned the following values: S_o=1368 Wm^{-2}, T_{atm}= 0.79 [25] N_{cloud} = 0.6 and the surface albedo and a = 0.22. although the model is simple, but, was used to provide reasonable estimates for the radiative forcing by both sulphate aerosols [5] and absorbing smoke aerosols [6].

The spectral behavior of the aerosols optical depth (τ). that expresses the spectral dependence of any of the optical parameters with the wavelength of light (λ) as inverse power law [1-2] is given by

$$\tau(\lambda) = \beta\lambda^{-\alpha} \quad (5)$$

The wavelength dependence of $\tau(\lambda)$ can be characterized by the Ångström parameter, which is a coefficient of the following regression:

$$ln\tau(\lambda) = -\alpha \ln(\lambda) + ln\beta \quad (6)$$

where β and α are the turbidity coefficient and Ångström exponent [22-23] α is related to the size distribution. The formula is derived on the premise that the extinction of solar radiation by aerosols is a continuous function of wavelength without selective bands or lines for scattering or absorption [27].

The Angstrom exponent itself varies with wavelength, and a more precise empirical relationship between aerosol extinction and wavelength is obtained with a 2nd-order polynomial [7-14] as:

$$ln\tau(\lambda) = \alpha_2(ln\lambda)^2 + \alpha_1 ln\lambda + ln\beta \quad (7)$$

The coefficient α_2 accounts for "curvature" often observed in Sun photometry measurements. In case of negative curvature ($\alpha_2 < 0$) while positive curvature ($\alpha_2 > 0$). [7] reported the existence of negative curvatures for fine mode aerosols and positive curvatures for significant contribution by coarse mode particles in the size distribution.

RESULTS AND DISCUSSION

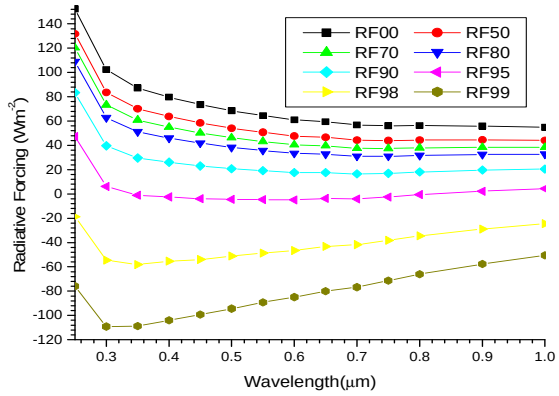

Figure 1a. A graph of radiatiive forcing against wavelength

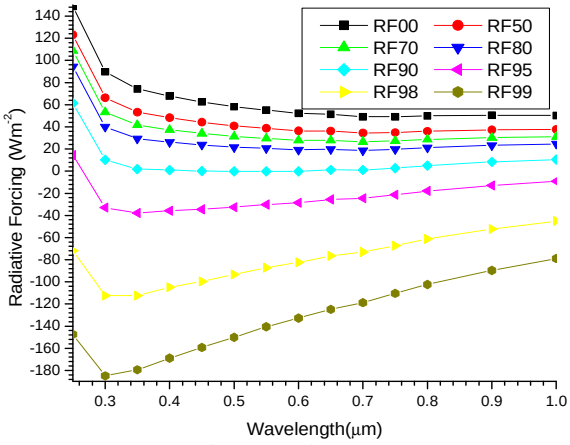

Figure 1b. A graph of radiative forcing against wavelength

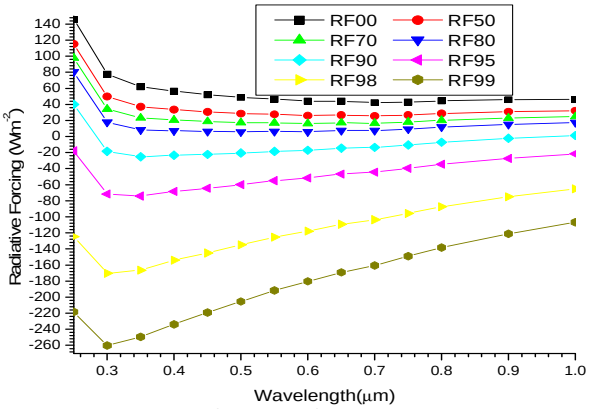

Figure 1c. A graph of radiative forcing against wavelength

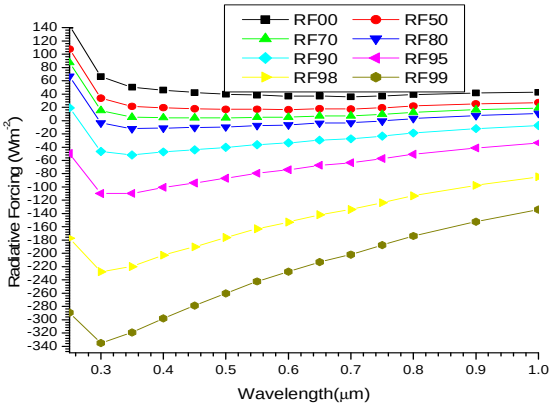

Figure 1d. A graph of radiative forcing against wavelength

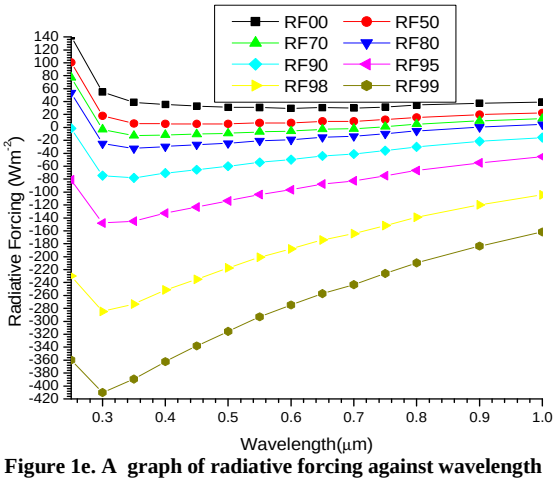

Figure 1e. A graph of radiative forcing against wavelength

In relation to wavelengths we observed that at 0% RH in Figure 1a shows that it is more dependent at shorter wavelength with sharp fall at 0.25 to 0.3 μm but from 0.3 to 1.0 μm it becomes almost a straight line with very small negative slope. As the RH increases from 50-99% RHs in Figure 1a and from 0-99% RHs from Figure 1b to Figure 1e the steepness decreases but at the spectral interval of 0.3 to 1.0 μm the slope continues to decrease and subsequently becomes positive. The overall effect is that there is a general decrease in RF at all RHs when compared from Figure 1a to Figure 1e attributing to cooling effect, this shows that water soluble due to high percentage of sulphate has a relatively high scattering coefficient.

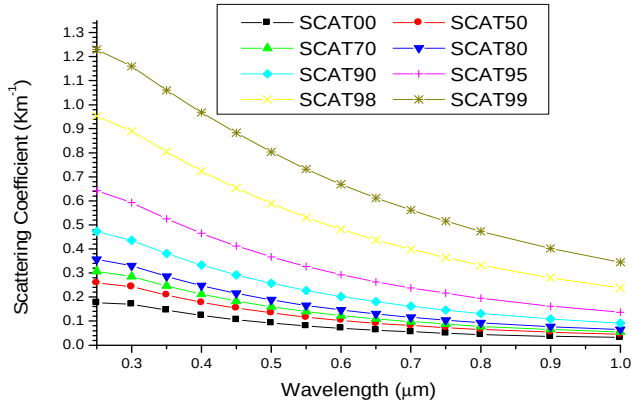

Figure 2a. A graph of scattering coefficient against wavelength

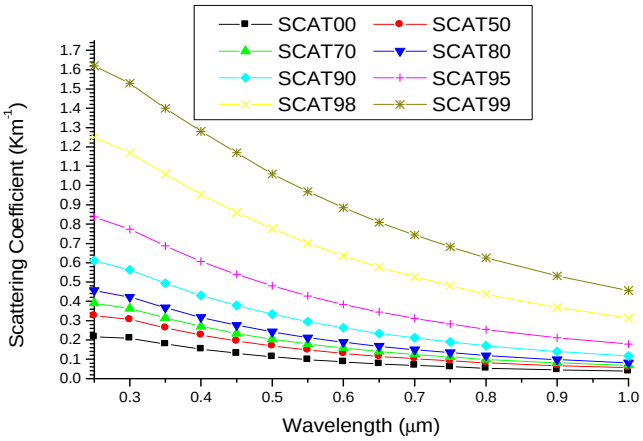

Figure 2b. A graph of scattering coefficient against wavelength

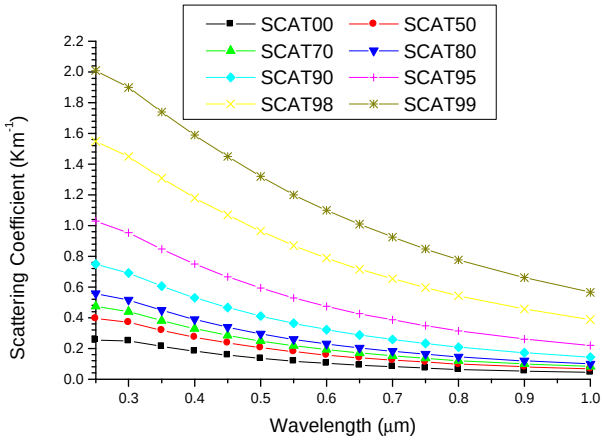

Figure 2c. A graph of scattering coefficient against wavelength

The scattering coefficients shown in Figure 2a to Figure 2e follow a relatively smooth decrease in wavelength at all RHs and can be approximated with power law wavelength dependence. It can be seen from the Figures that there is a relatively strong wavelength dependence of scattering coefficients at shorter wavelengths that gradually decreases towards longer wavelengths irrespective of the RH, attributing to the presence of both fine and coarse mode particles. The dominance of the higher concentration of the fine mode particles which are selective scatters enhances the irradiance scattering in shorter wavelengths only while the coarse mode particles provide similar contributions to the scattering coefficients at both wavelengths [29]. It also show that as a result of hygroscopic growth, smaller particles scatter more light at shorter wavelengths compared to bigger particles. The relation of scattering coefficients with RH is such that at the deliquescence point (90 to 99%) this growth with higher humidities increases

substantially, making the process strongly nonlinear with relative humidities [16]. The overall effect in general shows that the scattering coefficient increases at all RHs indicating cooling effect.

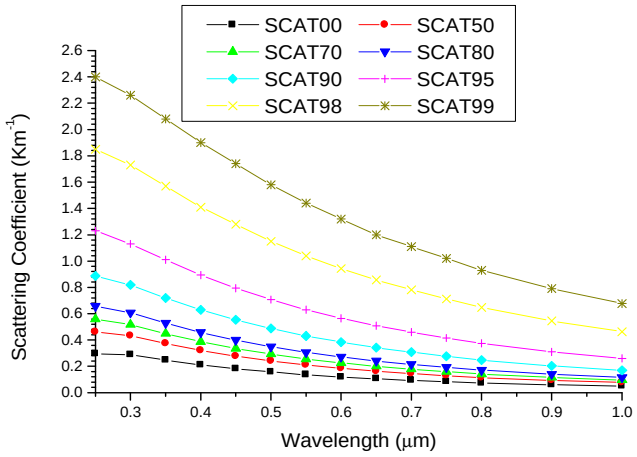

Figure 2d. A graph of scattering coefficient against wavelength

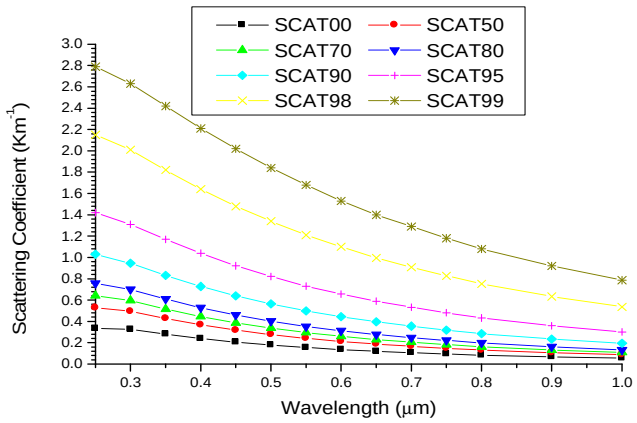

Figure 2e. A graph of scattering coefficient against wavelength

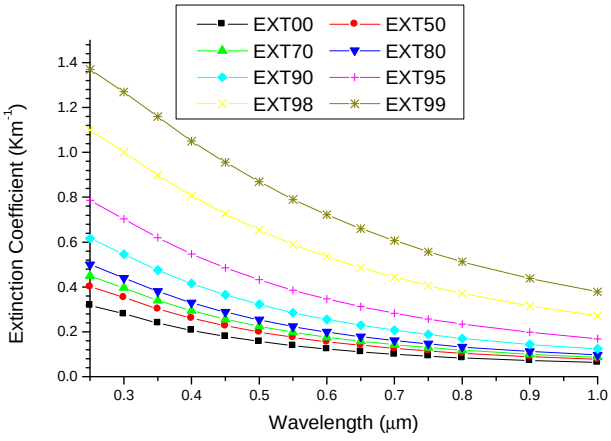

Figure 3a. A graph of extinction coefficient against wavelength

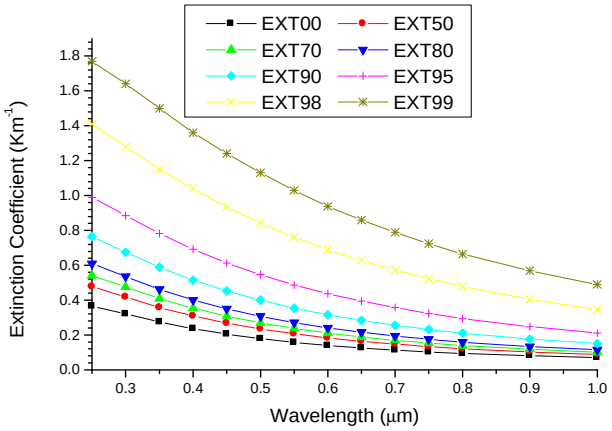

Figure 3b. A graph of extinction coefficient against wavelength

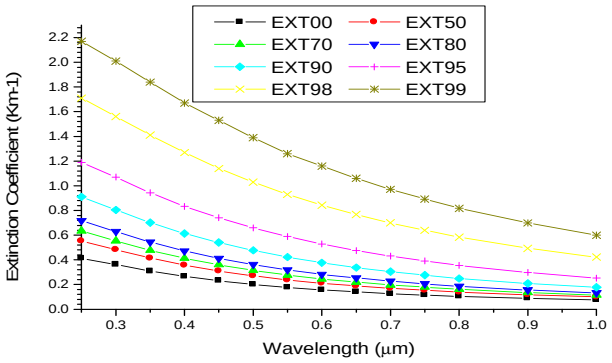

Figure 3c. A graph of extinction coefficient against wavelength

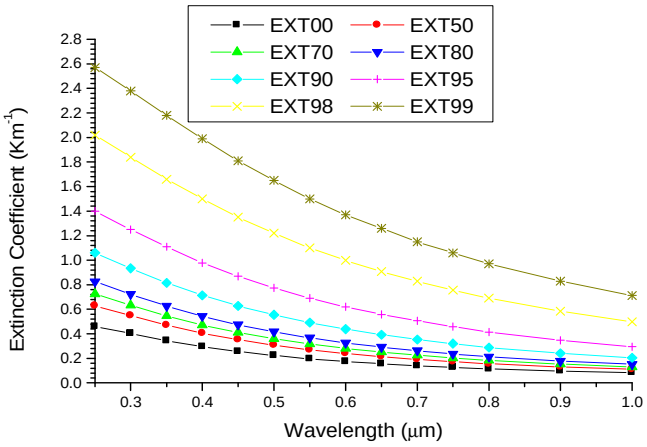

Figure 3d. A graph of extinction coefficient against wavelength

The extinction coefficient increases with increase in RHs. There is a relatively strong wavelength dependence of extinction coefficient at shorter wavelengths that gradually decreases towards the longer wavelength regardless of the RHs, attributing to the presence of both fine and coarse mode particles. The overall effect shows that from Figure 3a to Figure 3e there is an increase in extinction coefficient with RHs.

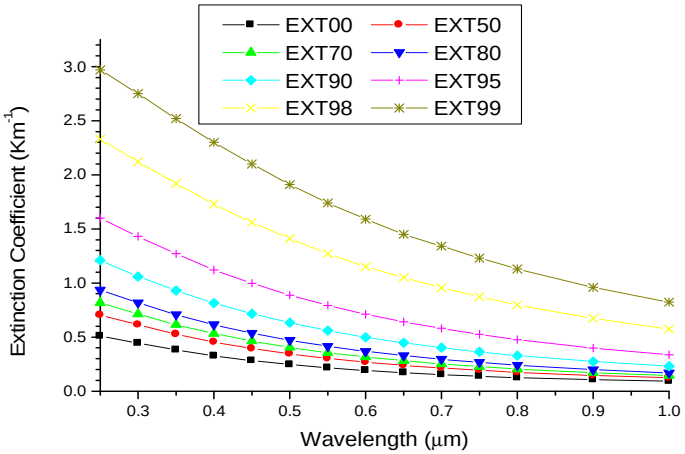

Figure 3e. A graph of extinction coefficient against wavelength

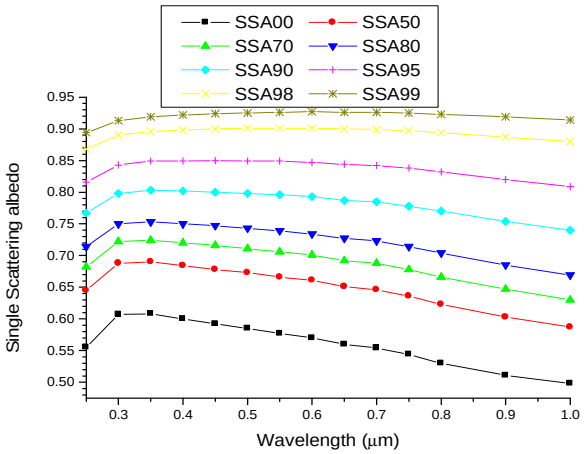

Figure 4a. A graph of single scattering albedo against wavelength

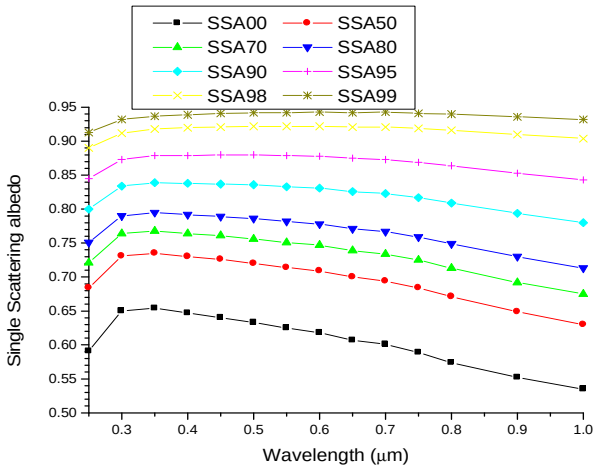

Figure 4b. A graph of single scattering albedo against wavelength

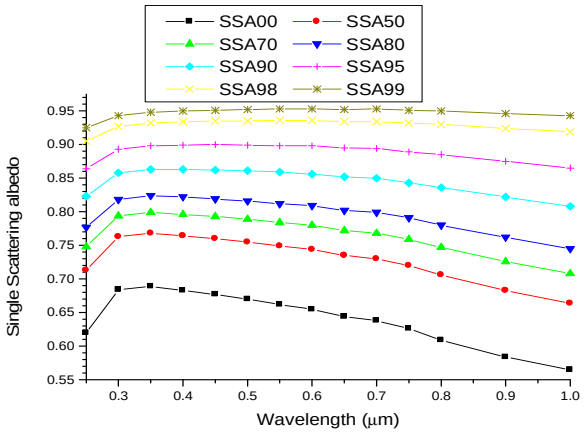

Figure 4c. A graph of single scattering albedo against wavelength

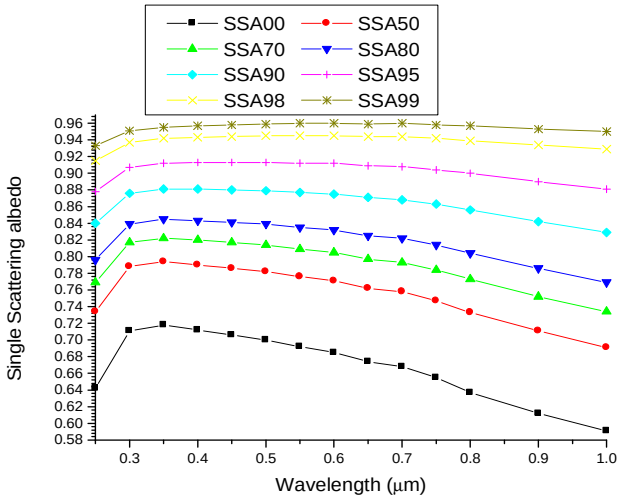

Figure 4d. A graph of single scattering albedo against wavelength

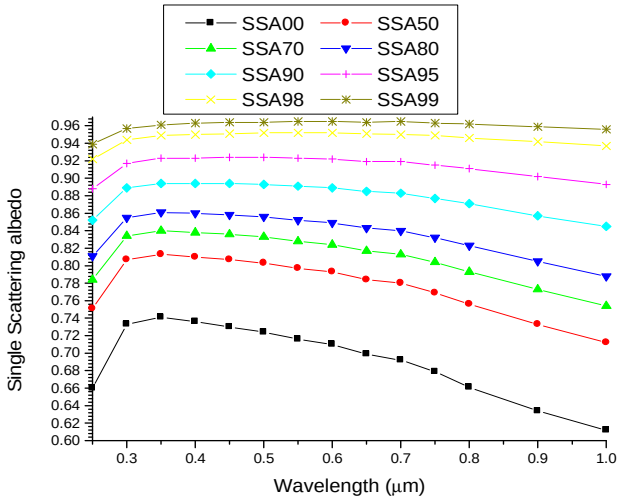

Figure 4e. A graph of single scattering albedo against wavelength

From Figure 4a to Figure 4e we observed that the single scattering albedo, ω_0, increases with increase in RH as a result of hygroscopic growth. The determination of optical parameters as a function of wavelength is useful to distinguish between different aerosols types. [15] reported that for urban industrial aerosols and biomass burning the ω_0 decreases with increasing wavelength, this effect is clearly observed in our Figures in which ω_0 decreases with increasing wavelength. There is a sharp initial increases in ω_0 which tend to decrease with wavelength at all RHs

given a positive slope and subsequently a negative slope. The overall effect shows that from Figure 4a to Figure 4e there is a general increase in ω_0 with RHs attributing that the aerosols has high scattering coefficient reflecting cooling effect.

Table 2: The results of α and α_2 for model 1 using equations (6) and (7) with SPSS 16.0

	LINEAR			QUADRATIC			
RH(%)	R^2	α	β	R^2	α_1	α_2	β
0	0.99715	0.90177	1.943251	0.99716	-0.8917	0.007389	1.94753
50	0.99760	0.96343	2.230815	0.99803	-1.03138	-0.04985	2.19799
70	0.99726	0.98463	2.422911	0.99836	-1.09634	-0.08194	2.36458
80	0.99664	0.99871	2.637723	0.99865	-1.15178	-0.11229	2.55110
90	0.99451	1.01104	3.196606	0.99910	-1.24570	-0.17214	3.03708
95	0.99070	0.99927	4.147965	0.99950	-1.32093	-0.23596	3.86687
98	0.98353	0.94394	6.263338	0.99980	-1.35874	-0.30429	5.72144
99	0.97745	0.88640	8.485223	0.99991	-1.34539	-1.34539	7.67674

Table 3: The results of α and α_2 for model 2 using equations (6) and (7) with SPSS 16.0

	LINEAR			QUADRATIC			
RH(%)	R^2	α	β	R^2	α_1	α_2	β
0	0.99747	0.94772	2.08209	0.99757	-0.97988	-0.02359	2.06753
50	0.99723	1.01163	2.46629	0.99842	-1.1313	-0.08778	2.40274
70	0.99652	1.03141	2.72223	0.99873	-1.1973	-0.12169	2.62548
80	0.99553	1.04280	3.00860	0.99897	-1.25241	-0.15376	2.87412
90	0.99286	1.04787	3.75312	0.99937	-1.33775	-0.21265	3.52312
95	0.98865	1.02660	5.01969	0.99967	-1.39685	-0.27161	4.63017
98	0.98133	0.94394	6.26334	0.99980	-1.35874	-0.30429	5.72144
99	0.97745	0.88640	8.48522	0.99991	-1.34539	-1.34539	7.67674

Table 4: **The results of α and α_2 for model 3 using equations (6) and (7) with SPSS 16.0**

	LINEAR			QUADRATIC			
RH(%)	R^2	α	β	R^2	α_1	α^2	β
0	0.99747	0.98621	2.22118	0.99790	-1.05609	-0.05126	2.18757
50	0.99664	1.04948	2.70245	0.99870	-1.21245	-0.11955	2.60806
70	0.99568	1.06714	3.02241	0.99898	-1.27704	-0.15398	2.88713
80	0.99449	1.07622	3.37934	0.99920	-1.3292	-0.18558	3.19789
90	0.99149	1.07453	4.30959	0.99952	-1.40489	-0.24234	4.00992
95	0.98707	1.04544	5.89165	0.99976	-1.45039	-0.29706	5.39349
98	0.97978	0.96941	9.41156	0.99993	-1.44428	-0.34835	8.48535
99	0.97371	0.90115	13.11354	0.99997	-1.40667	-0.37084	11.74421

Table 5: **The results of α and α_2 for model 4 using equations (6) and (7) with SPSS 16.0**

	LINEAR			QUADRATIC			
RH(%)	R^2	α	β	R^2	α_1	α_2	β
0	0.99726	1.01868	2.36092	0.99813	-1.12123	-0.07522	2.30869
50	0.99602	1.08026	2.93870	0.99891	-1.27885	-0.14568	2.81410
70	0.99486	1.09529	3.32283	0.99916	-1.34138	-0.18052	3.14914
80	0.99352	1.10162	3.75116	0.99935	-1.39000	-0.21154	3.52244
90	0.99043	1.09465	4.86592	0.99963	-1.45508	-0.26440	4.49797
95	0.98598	1.05941	6.76225	0.99983	-1.48834	-0.31466	6.15817
98	0.97864	0.97662	10.98435	0.99995	-1.46895	-0.36116	9.86572
99	0.97264	0.90531	15.42577	0.99998	-1.42381	-0.38035	13.77596

Table 6: **The results of α and α_2 for model 5 using equations (6) and (7) with SPSS 16.0**

	LINEAR			QUADRATIC			
RH(%)	R^2	α	β	R^2	α_1	α_2	β
0	0.99696	1.04656	2.50082	0.99833	-1.17915	-0.09726	2.42952
50	0.99541	1.10595	3.17485	0.99906	-1.33480	-0.16788	3.02024
70	0.99410	1.11844	3.62298	0.99929	-1.39437	-0.20242	3.41133
80	0.99271	1.12238	4.12245	0.99947	-1.43883	-0.23214	3.84745
90	0.98947	1.11037	5.42266	0.99970	-1.49617	-0.28301	4.98493
95	0.98501	1.06995	7.63376	0.99986	-1.51877	-0.32924	6.92174
98	0.97777	0.98183	12.55922	0.99996	-1.48721	-0.37074	11.24812
99	0.97188	0.90820	17.74123	0.99999	-1.43583	-0.38705	15.81226

According to [7-8] and [27] positive values of Ångström exponent α are characteristics of fine-mode-dominated aerosols size distributions while near zero and negative values are characteristics of dominant coarse-mode or bi-modal size distributions, with coarse-mode aerosols having significant magnitude. Comparing Tables 2, 3, 4, 5 and 6. The Ångström exponent, α, reflects the dominance of fine mode particles at all RHs. However, in Tables 2 and 3 α increases from 0-90%RHs and decreases from 95-99% RHs but, in Tables 4, 5 and 6 α increases from 0-80% RHs and decreases from 90-99% RHs. The curvature, α_2, in Table 2 at 0% RH reflects the dominance of coarse mode particles but from 50-99% RHs reflects fine mode particles which verified α In Table 3, 4, 5 and 6 α_2 reflects the dominance of fine particles at all RHs which verified α In Tables 2, 3, 4, 5 and 6 the turbidity, β, increases with increase in RHs from 0-99% RHs in both the linear and quadratic part of the regression analysis. The overall effect is that the fine mode particles are dominant compared to coarse mode particles.

CONCLUSION

From our results, the RF (cooling) decreases at all RHs. The scattering and extinction coefficients increases at all RHs attributing the dominance of water soluble reflecting cooling effect. The values of the Ångström exponents and curvatures indicates the dominance of fine mode particles and are comparable to those found in pollution outbreaks in the Northern Asian region [3]. The observed increase in scattering, which tends to be much more greater than the absorption indicates that hygroscopic growth has more effect on the fine mode particles than the coarse mode at the spectral range of 0.25-1.00 μm and that is what is responsible for the radiative cooling. This shows that water soluble components which contains large percentage of sulphate and also contain nitrate has a relatively high scattering coefficient.

In this study, the single scattering albedo, ω_0 increases with RH and decrease in wavelength. [15] Reported that for urban industrial aerosols and biomass burning the ω_0 decreases with increasing wavelength, our analysis shows that the decrease in ω_0 with increasing wavelength is more as the RHs decreases. We calculated the ω_0 for the analysis of water soluble and obtained values ranging from 0.55 to 0.94 at spectral range of 0.25-1.00 μm.

REFERENCES

[1] A. Ångström, *Geografiska Annaler*, **1929,** 11, 156-166.
[2] A. Ångström, *Tellus*, **1961,** 13(2), 214-223.
[3] A. Ansmann, R. Engelmann, D. Althausen, U. Wandinger, M. M. Hu, and Y. Zhang, *Geophysical Research Letters*, **2005,** 32, L13815.
[4] O. Boucher,and J. Haywood, *Clim. Dynam*, **2001,** 18, 297-302
[5] R. J. Charlson, S. E. Schwartz, J. M. Hales, R. D. Cess, J. A. Coakley, J. E. Hansen, and D. J. Hoffmann, *Science*, **1992,** 255, 423-430.
[6] P. Chylek, and J. Wong, *Geophysical Research Letters*, **1995,** 22, 929-931
[7] T. F. Eck, B. N. Holben, J. S. Reid, O. Dubovik, A. Smirnov, N. T. O'Neill, I. Slutsker, and S. Kinne, *Journal of Geophysical Research*, **1999,** 104, 333-349.
[8] T. F. Eck, B. N. Holben, O. Dubovic, A. Smirnov, I. Slutsker, J. M. Lobert, and V. Ramanathan, *Journal of Geophysical Research*, **2001a,** 106, 28,555-28,566.
[9] T. F. Eck, B. N. Holben, D. E. Ward, O. Dubovik, J.S. Reid, A. Smirnov, M.M. Mukelabai, N.C. Hsu, N.T. O'Neill, and V. Ramanathan, *Journal of Geophysical Research*, **2001b,** 106, 3425-3448.
[10] T. F. Eck, B. N. Holben, D. E. Ward, O. Dubovik, J. S. Reid, A. Smirnov, M. M. Mukelabai, N. C. Hsu, N. T. O'Neill, and I. Slutsker, *Journal of Geophysical Research*, **2003,** 106, 3425-2448.
[11] Y. Kaufman, *Journal of Geophysical Research*, **1993,** 98 (D2), 2677-2692.
[12] M. King and D. Byrne, *Journal of Geophysical Research*, **1976,** 33, 3251-3254.
[13] N. T. O'Neill, O. Dubovik, and T. F. Eck, *Appl. Opt* , **2001,** 40 (15), 2368-2375.
[14] N. T. O'Neill, T. F. Eck, A. Smirnov, B. N. Holben, and S. Thulasiraman, *Journal of Geophysical Research*, **2003,** 108 (D17), 4559.
[15] O. Dubovik, B. Holben, T. Eck, A. Smirnov, Y. Kaufman, M. King, D. Tanre, and I. Slutsker, *J. Atmos Sci*, **2002,** 59, 1135-1150.
[16] J. W. Fitzgerald, *Journal of Applied Meteorology*, **1975,** 14, 1044-1049
[17] J. M. Haywood, and K.P. Shine, *Journal of Geophysical Research, Lett*, **1995,** 22(5), 603-606.
[18] J. M. Haywood, D. L. Roberts, A. Slingo, J. M. Edwards, and K. Shine *Journal of climate*, **1997,** 10, 1562-1577.
[19] D. Muller, U. Wandinger, and A. Ansmann, *Appl opt*, **1999,** 38, 1981-1999.
[20] D. A. Hegg, P.V. Hobbs. S. Gasso, J. D. Nance, and A. L. Rango, *Journal of Geophysical Research*, **1996,** 101, 23349-23363.

[21] M. Hess, P. Koepke, and I. Schult, Optical Properties of Aerosols and Clouds. American Meteorology Society. **1998,** 831-844.
[22] K. N. Liou, An introduction to Atmospheric Radiation 2nd ed. Academic, San Diego, California. **2002**
[23] N. T. O'Neill, and A. Royer, *Appl. Opt*, **1993,** 32, 1642-1645
[24] H. Moosmuller, R. K. Chakrabarty, and W. P. Arnott, *A review, J. Quant Spectrosc. R*, **2009,** 110, 844-878.
[25] J. E. Penner, R. E. Dickinson,and C. A. O'Neill, *Science*, **1992,** 256, 1432-1434.
[26] V. Ramanathan, P. J. Crutzen, and J. Lelievld, *Journal of Geophysical Research*, **2001,** 106, 28371-28398.
[27] R. R. Ranjan, H. P. Joshi, and K. N. Iyer, *Aerosol and Air Quality Research*, **2007,** 7, 33-45
[28] C. Sagan, and J. Pollack, *Journal of Geophysical Research*, **1967,** 72, 469-477.
[29] G. L. Schuster, O. Dubovik, and B. N. Holben, *Journal of Geophysical Research*, **2006,** 111, 72-97.